INSTITUTE FOR FUSION STUDIES

DOE/ET-53088-422 IFSR #422

Particle Simulation Model of the Lorentz Collision Operator in Guiding-Center Plasmas

J.H. Han
Institute for Fusion Studies
The University of Texas at Austin
Austin, Texas 78712
and
J.-N. Leboeuf
Oak Ridge National Laboratory
P.O. Box 2009
Oak Ridge, TN 37830

March 1990

THE UNIVERSITY OF TEXAS

AUSTIN

Particle Simulation Model of the Lorentz Collision Operator in Guiding-Center Plasmas

J.H. Han
Institute for Fusion Studies
The University of Texas at Austin
Austin, Texas 78712
and
J-N. Leboeuf
Oak Ridge National Laboratory
P.O. Box 2009
Oak Ridge, TN 37830

Abstract

A simulation model of the Lorentz collision operator has been developed for guiding-center electron plasmas. This model conserves the energy and magnetic moment μ of the magnetized electrons. Tests of this model have been carried out for low frequency electrostatic resistive interchange modes in sheared slab geometry by using a $2-\frac{1}{2}$D guiding-center particle code. Comparisons with linear theory results from a second order shooting code give good agreement in growth rates and mode widths.

I. Introduction

In particle simulations of low frequency plasma instabilities, guiding-center electron plasma models[1,2] are used to eliminate unnecessary high frequency electron cyclotron oscillations. This means that only the thermal velocity along the ambient magnetic field is kept for the electrons in the simulation model, instead of the full three-directional thermal velocities as is done in conventional particle codes. In guiding-center electron models, the perpendicular electron velocities only come in as particle drift velocities, such as $\mathbf{E} \times \mathbf{B}$, $g \times \mathbf{B}$ or diamagnetic drifts due to pressure gradients. These perpendicular electron velocities due to particle drifts are also much smaller than the electron thermal velocity for relevant simulation parameters.

The guiding-center electron model uses the predictor-corrector method[2] to accurately advance the electron velocities and positions in time. This is necessary since the electrons respond instantaneously to the electric field in the perpendicular direction, while parallel electron acceleration is retained. The ions are pushed using the standard leapfrog scheme with full three-directional velocities and Lorentz force, thus allowing for finite ion gyro-radius effects.

When collisionality is introduced in this guiding-center electron plasma model by adopting the Lorentz gas model for the collision operator,[3,4] we face a mismatch between these two models. The Lorentz collision operator allows the particles to do small pitch-angle scattering in three-dimensional velocity space, conserving each particle's energy but not its momentum. Each particle velocity vector changes its direction after each small pitch-angle scattering process, all the while preserving its magnitude. The Lorentz collision model requires three velocities which are the same order of magnitude to perform the right amount of scattering. On the other hand, the guiding-center electron model only evolves the parallel

electron thermal velocity and neglects perpendicular thermal velocities which would generate high frequency electron cyclotron waves.

Several consecutive pitch-angle scattering processes with only one significant velocity component will cause a significant loss of its magnitude. Therefore the particle energy conservation during the collisional process, which is the character of the Lorentz collision operator, cannot be maintained in the guiding-center electron plasma model. As a cure for this problem, we make use of the conservation of the magnetic moment μ and introduce, during the collisional process, two perpendicular pseudo-thermal electron velocity components in addition to the parallel electron thermal velocity component. We, however, retain only that same parallel electron thermal velocity after collision and the two perpendicular velocity components due to particle drifts in the dynamical part of the simulation procedure. So doing, we can achieve particle energy conservation for the collisional parallel electron dynamics and retain the low frequency character of the guiding-center electron plasma model.

We have applied this collisional model to the case of low frequency electrostatic resistive interchange modes in sheared slab geometry. A $2-\frac{1}{2}$ D electrostatic particle code with this particular implementation of the Lorentz collision operator is used to simulate these modes. Agreement between simulation and theory is good in terms of linear growth rates and linear eigenmode widths.

II. Implementation of the Lorentz Collision Operator in Guiding-Center Electron Plasma Models

The Lorentz collision operator, which conserves particle energy and number density, is defined by

$$C(g_e) = \frac{\nu_{ei}}{\sin\theta}\frac{\partial}{\partial\theta}\left[\sin\theta\left(\frac{\partial g_e}{\partial\theta}\right)\right] \tag{1}$$

where g_e is the adiabatic part of the electron distribution function. Other definitions are :

$$\theta = \cos^{-1}\left(\frac{v_{\|}}{(v_{\|}^2 + v_{\perp}^2)^{1/2}}\right) : \quad \text{pitch angle}$$

$$\nu_{ei} = 2\pi n_0 e^4 \ln\Lambda/(m_e^2 v_{Te}^3) : \quad \text{collision frequency}$$

It is clear that this collision operator cannot be implemented straightforwardly in the guiding-center electron model which has only one electron thermal velocity component parallel to the sheared equlibrium magnetic field $\mathbf{B}_0 = B_0\left(\mathbf{z} + \left(\frac{x - x_0}{L_s}\right)\mathbf{y}\right)$. The reason is due to the fact that the electron parallel velocity at $t = \Delta t$ after a small pitch-angle scattering process will be

$$v_{\|}(\Delta t) = v_{\|}(t = 0) \times \cos\theta \tag{2}$$

and then after n time steps ($t = n\Delta t$), the electron parallel velocity begins to lose most of its magnitude due to this scattering:

$$v_{\|}(n\Delta t) = v_{\|}(t = 0) \times (\cos\theta)^n \ll 1 \ . \tag{3}$$

Therefore if the Lorentz collision operator is implemented in a guiding-center particle code without considering the conservation of particle energy, the parallel electron maxwellian velocity distribution rapidly becomes a cold electron beam due to the scattering process of Eq. (3) as shown in Fig. 1. The gains or losses in magnitude by the perpendicular velocities are, however, not propagated by the dynamics, since these are recalculated from the appropriate particle drifts at each time step.

To resolve the problems caused by this parallel guiding-center electron velocity loss in the Lorentz collision model, two pseudo-thermal perpendicular electron velocities, which are randomly generated from a Maxwellian (at $t = 0$), are introduced to conserve electron energy E,

$$E = \frac{1}{2} m_e v_{\|}^2 + \mu B_0 + e\phi_0$$

and electron magnetic moment μ, which is the adiabatic invariant of the guiding-center electron,

$$\mu = \frac{m_e v_\perp^2}{2B_0} \ .$$

These two electron pseudo-thermal perpendicular velocities are used only in the scattering process and do not propagate into the perpendicular electron dynamics. By performing the collisional procedure in the manner detailed next, the conservation of parallel guiding-center electron energy during the collision is recovered (Fig. 2).

At t = 0

Guiding-center electrons having

$$E = \frac{1}{2} m_e \, v_\parallel^2 + \mu B_0 + e\Phi_0 = \text{ const. } ,$$

$$\mu = m_e v_\perp^2 / 2B_0 = \text{ const.}$$

are loaded and three thermal electron velocities

$$\left(v_\parallel, v_{\perp 1}, v_{\perp 2}\right)$$

are defined with $v_\perp^2 = v_{\perp 1}^2 + v_{\perp 2}^2$.

Scattering by Lorentz Collision Operator

$$\Delta\theta_j = \left[-4\nu_{ei} \left(\frac{v_{Te}}{(v_\parallel^2 + v_\perp^2)^{1/2}} \right)^3 \Delta t \, \ln(1 - r_j) \right]^{1/2}$$

$$r_j = (0,1) \quad ; \quad \text{random number } \Delta t; \text{ time step.}$$

At t = Δt:

The velocity gains or losses generated by the collisional process are

$$(\Delta v_\parallel, \Delta v_{\perp 1}, \Delta v_{\perp 2}) \ .$$

These velocity increments are added to the old velocity set before scattering and updated as a new velocity set which will be used as input for the electron thermal velocities at the next time step.

$$v_{\|}^{\text{new}} = v_{\|}^{\text{old}} + \Delta v_{\|}$$

$$v_{\perp 1}^{\text{new}} = v_{\perp 1}^{\text{old}} + \Delta v_{\perp 1}$$

$$v_{\perp 2}^{\text{new}} = v_{\perp 2}^{\text{old}} + \Delta v_{\perp 2} \ .$$

The Δv's used are explicitly given in the Appendix.

III. Application: Electrostatic Resistive Interchange Modes in Sheared Slab Geometry

We have applied the Lorentz collision model to simulate electrostatic resistive interchange modes in sheared slab geometry.[5] In this model, the centrifugal force due to magnetic curvature is represented by T_e/L_c for electrons and T_i/L_c for ions respectively. One should note that the ratio of curvature drift between electrons $\frac{cT_e}{eB_0}\frac{1}{L_c}$ and ions $-\frac{cT_i}{eB_0}\frac{1}{L_c}$ depends on T_e/T_i rather than m_e/m_i as in the case of a gravitational interchange instability.

A resistive interchange mode driven by the pressure gradient is localized at the resonant surface ($k_{\|} = k_y x/L_s = 0.0$). The plasma is decoupled from the field lines there and can become unstable with a small amount of resistivity. We are looking for this mode in the near fluid regime for which

$$\text{Re}(\omega) < \omega_e^* \quad \text{and} \quad \gamma = \left(\frac{\nu_{ei}\, L_s^2}{\tau\, k_y^2\, \rho_i^2\, v_{Te}^2}\right)^{1/3} \left[\omega_e^*\, \omega_{de}\left(1 + \frac{1}{\tau}\right)\right]^{2/3} , \tag{4}$$

yet retain kinetic ingredients such as finite ion larmor radius and ω_e^* effects. The growth rate expression in Eq. (4) is obtained from the following analysis.

Linear analysis is carried out by solving the linear eigenmode equation derived from kinetic theory to obtain plausible parameters for the simulations. Since the number conserv-

ing Krook collision operator and the Lorentz collision operator produce equivalent results for interchange modes,[6] we use this number conserving Krook operator in linear theory calculations for simplicity.

The linear eigenmode equation for electrostatic resistive interchange modes is derived from the linearized drift-kinetic equation for the guiding-center electrons

$$(\omega - \omega_{de} - k_{\|} v_{\|e}) g_e - i\, C(g_e) = -\left(\frac{|e|}{T_e}\right) F_e^M (\omega - \omega_e^*) \Phi \ ,$$

where

$$\omega_{de} = \frac{cT_e}{eB_0} \frac{k_y}{L_c} \ , \qquad \omega_e^* = \frac{cT_e}{eB_0} \frac{k_y}{L_n}$$

and

$$C(g_e) = -\nu_{ei} \left[g_e - \frac{F_e^M}{n_0} \int d^3v\, g_e \right]$$

is the number conserving Krook collision operator[6] with perturbed electron distribution function

$$f_e = \frac{e}{T_e} \Phi\, F_e^M + g_e \ .$$

The linearized gyro-kinetic equation describes the behavior of the ions with finite Larmor radius ρ_i

$$(\omega - \omega_{di} - k_{\|} v_{\|i}) g_i = \left(\frac{|e|}{T_i}\right) F_i^M (\omega - \omega_i^*) J_0(k_\perp \rho_i)$$

with

$$f_i = \left(\frac{|e|}{T_i}\right) \Phi F_i^M + g_i e^{-iL}, \ L = k_\perp \rho_i \cos\varphi$$

$$\omega_{di} = -\omega_{de}/\tau, \quad \omega_i^* = -\omega_e^*/\tau, \quad \tau = T_e/T_i \ .$$

Averaging f_e and f_i over the velocity space yields n_e and n_i. By invoking quasi-neutrality,

$n_e \sim n_i$, we obtain the eigenmode equation for the perturbed electrostatic potential Φ

$$\left[1+\tau+\left(\frac{\tau\omega+\omega_e^*}{\sqrt{2}\,k_{\|}v_{Ti}}\right)Z_i\left(\Gamma_0-\rho_i^2\frac{d\Gamma_0}{db}\frac{\partial^2}{\partial x^2}\right)\right.$$

$$\left.+\left(\frac{\omega-\omega_e^*}{\sqrt{2}\,k_{\|}v_{Te}}\right)Z_e\Big/\left(1+i\left[\frac{\nu_{ei}\,Z_e}{\sqrt{2}\,k_{\|}v_{Te}}\right]\right)\right]\Phi=0 \tag{5}$$

$$Z_e=Z_e(\xi_e),\xi_e=\frac{\omega-\omega_{de}+i\nu_{ei}}{\sqrt{2}\,k_{\|}v_{Te}}$$

$$Z_i=Z_i(\xi_i),\xi_i=\frac{\omega-\omega_{di}}{\sqrt{2}\,k_{\|}v_{Ti}}\ ,\qquad \Gamma_0=e^{-b}\,I_0(b)\ ,\ b=k_\perp^2\,\rho_i^2\ .$$

By expanding electron and ion Z-functions in the large argument limit we recover the expression for the growth rate of Eq. (4).

This eigenmode equation Eq. (5), normalized such that $x=x/\rho_i$ and $\omega=\omega/\omega_e^*$, is solved with a 2nd-order shooting code. Results of such linear calculations are shown in Fig. 3 and Fig. 4. The parameters used are $T_e/T_i=1.0$, $m_i/m_e=400$, $k_y\,\rho_i=0.098$, $L_s/L_n=14$, $L_n/L_c=0.134$, $\omega_e^*=3.436\times10^{-4}\,\omega_{pe}$ and $\omega_{ci}=0.05\omega_{pe}$. The collision frequency ν_{ei} is varied from 0 to values for which mode width and growth rate are nearly saturated (Fig. 3).

A $2-\frac{1}{2}$D bounded, electrostatic, guiding-center electron particle model[5,7] is used for the simulations. The configuration for this model is shown in Fig. 5. The single mode rational surface is located at x_0 in the middle of the sheared slab which is extended in the (x,y)-plane with conducting wall boundaries in the x-direction and periodic boundaries in the y-direction. Interchange parity, in which electrostatic potential Φ has even parity, is imposed at the mode rational surface. The method-II reflecting boundary scheme of Naitou *et al.*[8] is used to handle the particles at the walls. Simulations are carried out to measure the growth rate and mode width for comparison with the linear theory results. The simulation parameters used are the same as for the linear theory calculation with system sizes $L_x=64\Delta$, $L_y=128\Delta$, particle sizes $a_x=a_y=1.5\Delta$, $\rho_i=2\Delta$, $n_0=16/\Delta^2$, with unit grid

spacing Δ, $\rho_i/L_n = 0.14$, $\rho_i/L_c = 1.876 \times 10^{-2}$ and run time $(n\Delta t) = 4000 \times 4 = 800\omega_{ci}^{-1}$. The collision frequency ν_{ei} is varied from 0 to $160\omega_e^*$, which puts the growth rate in the $\gamma \sim \gamma_{ei}^{1/3}$ scaling range as shown in Fig. 4. As resistivity increases, quasilinear flattening of the density gradient commensurate with the broader mode width is observed (Fig. 6). The global electrostatic energy and its saturation level also increase more with increasing resistivity as shown in Fig. 7. Comparisons of growth rates and mode widths between simulation and theory are illustrated in Figs. 8 and 9. Although simulation and theory use different collision operators, the Lorentz collision operator and the number conserving Krook collision operator respectively, the degree of agreement is well inside the error bars. It is also well within what can be expected from the (shearless) linear theory results of Ref. 6 over the range of $\nu_{ei}/k_{\|}v_{Te}$ values used in the case of interchange modes.

IV. Summary

A Lorentz collision operator, which conserves particle energy and magnetic moment in magnetized plasmas, has correctly been implemented in the guiding-center electron particle simulation model, which is used to investigate low frequency plasma instabilities. This model has been applied to the electrostatic resistive interchange mode. It has reproduced the main features of this mode such as the $\gamma \sim \nu_{ei}^{1/3}$ growth rate scaling which prevails in the fluid limit and the typical mode structures which are observed in the linear eigenmode analysis. Further detailed study of resistive interchange mode in both electrostatic and electromagnetic limits using this collision model will be reported in future work.

Acknowledgment

We thank Dr. G.S. Lee and Dr. N. Dominguez for valuable discussions and comments. This work is supported by the U.S. Department of Energy contracts DE-FG05-80ET-53088 and DE-AC05-84OR-21400.

Appendix —Implementation of the Lorentz collision operator in particle codes

The Lorentz collision operator is implemented by considering each velocity component before and after collision. Let us define the velocity $\mathbf{v} = (v_x, v_y, v_z)$ in terms of angles P and T shown in Fig. A-1.

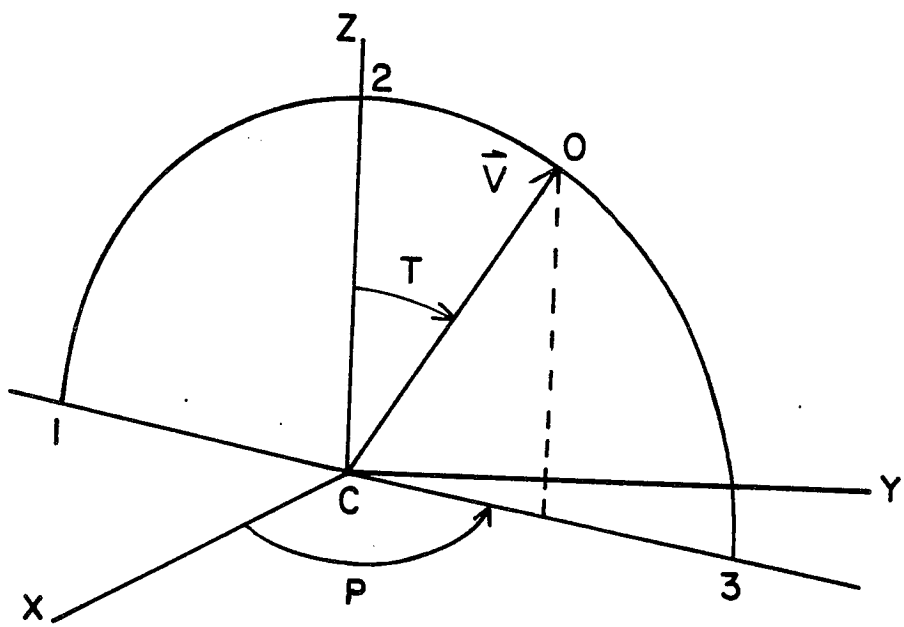

Fig. A-1

In this figure, velocities are defined as

$$v_x = v \sin T \cos P$$

$$v_y = v \sin T \sin P$$

$$v_z = v \cos T \ .$$

After scattering with pitch angle ϕ, the scattered velocity $\mathbf{v}'$ will be located at the arbitrary point A on the circle centered at O' with radius $R = v \sin\phi$, as shown in Fig. A-2. Now $\mathbf{v}' = CA$ is separated into $O'A$ and CO', which is perpendicular and parallel to $\mathbf{v}$ respectively. On the circle centered at O' with radius R we can define another velocity set $(v'_{\|}, v'_{\perp 1}, v'_{\perp 2})$ with respect to the semicircle 1-2-3, passing through the center of circle O' in Fig. A-3. Thus the scattered velocity $\mathbf{v}'$ is expressed in the frame of $\mathbf{v}$ as

$$\mathbf{v}' = (v\cos\phi, v\sin\phi\cos\psi, v\sin\phi\sin\psi) \ .$$

By transforming $(v'_{\|}, v'_{\perp 1}, v'_{\perp 2})$ into (v'_x, v'_y, v'_z) we can calculate the velocity gain or loss for the scattered velocities in x, y, z coordinate p i.e.,

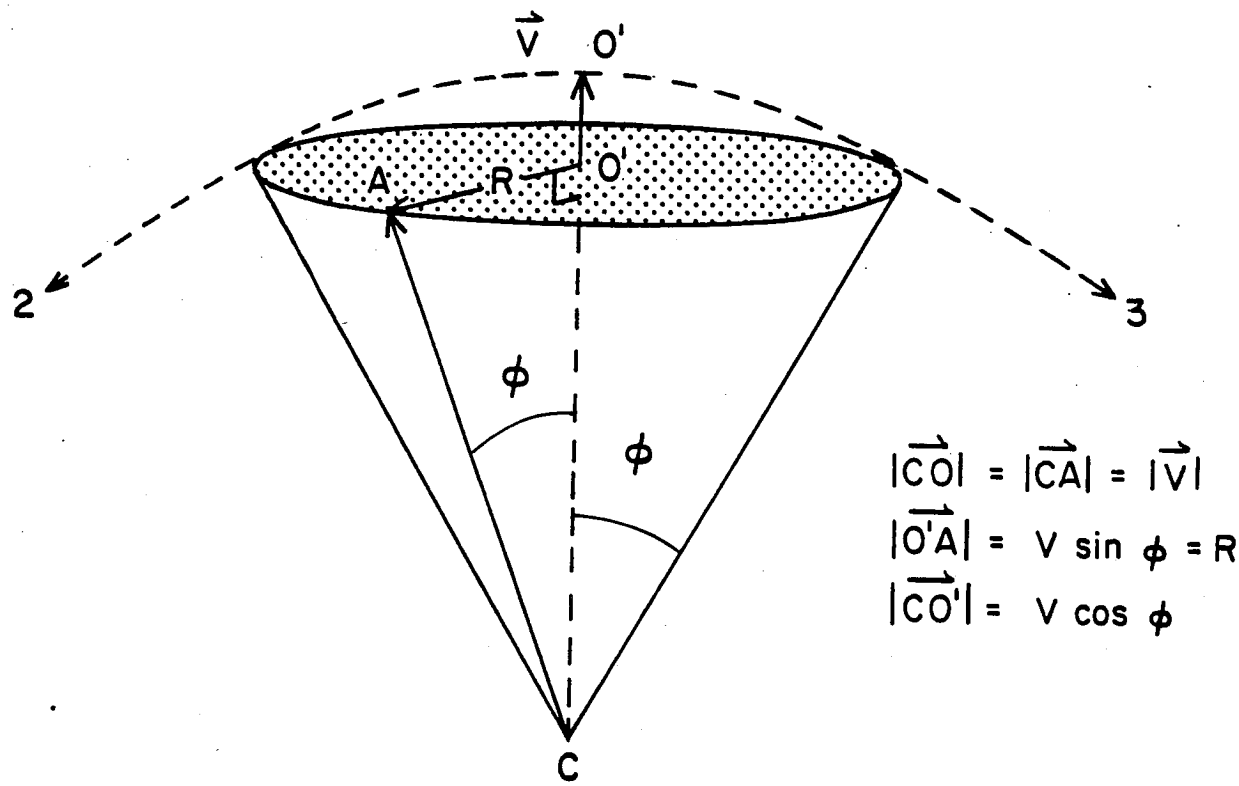

Fig. A-2

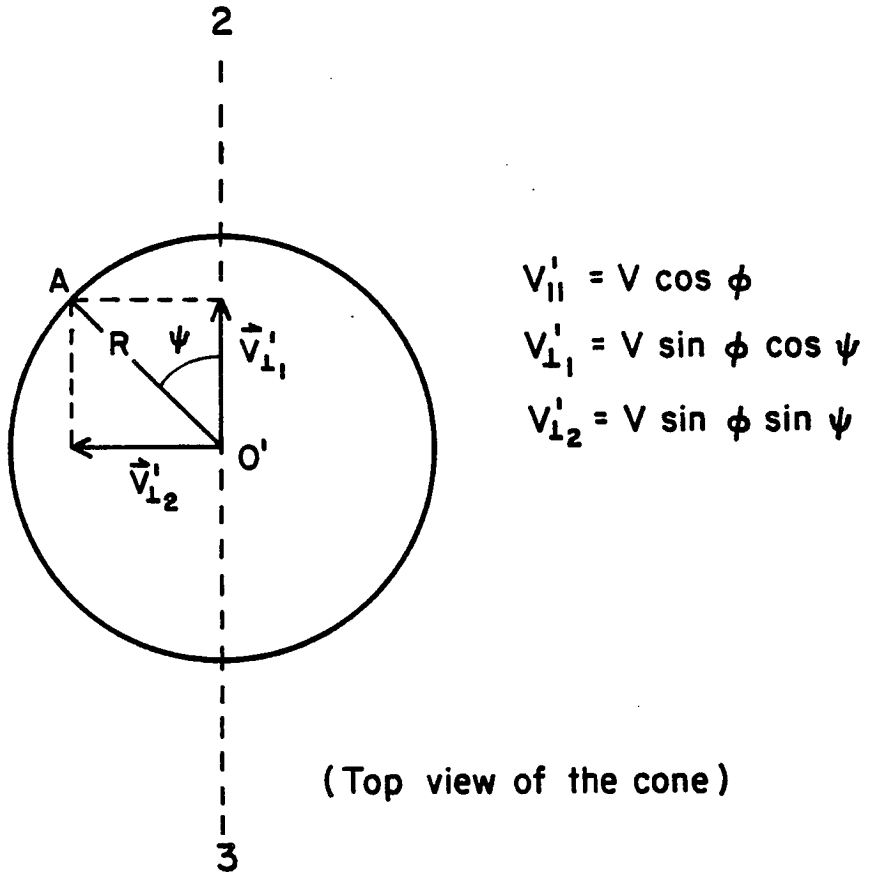

Fig. A-3

$$\Delta v_x = v'_x - v_x$$

$$\Delta v_y = v'_y - v_y$$

$$\Delta v_z = v'_z - v_z \ .$$

The projection of $v'_{\parallel}, v'_{\perp 1}, v'_{\perp 2}$ onto the x, y, z coordinates is shown with diagrams in Fig. A-4. From the diagrams in Fig. A-4 we can derive the contribution from ($\mathbf{v}'_{\parallel}$, $\mathbf{v}'_{\perp 1}$, $\mathbf{v}'_{\perp 2}$) to ($\mathbf{v}'_{\mathbf{x}}$, $\mathbf{v}'_{\mathbf{y}}$, $\mathbf{v}'_{\mathbf{z}}$). The projection of $\mathbf{v}'$ onto v_x (Fig. A-5) is

$$[\mathbf{v}'_{\parallel}]_{\mathbf{x}} = v \cos \phi \sin T \cos P$$

$$[\mathbf{v}'_{\perp 1}]_{\mathbf{x}} = v \sin \phi \sin \psi \sin P$$

$$[\mathbf{v}'_{\perp 2}]_{\mathbf{x}} = -v \sin \phi \cos \psi \cos T \cos P \ .$$

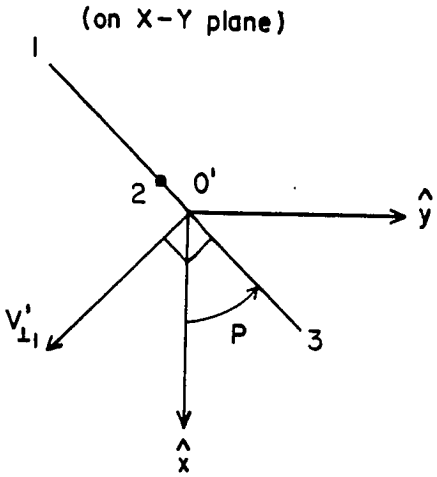

Fig. A-4-a

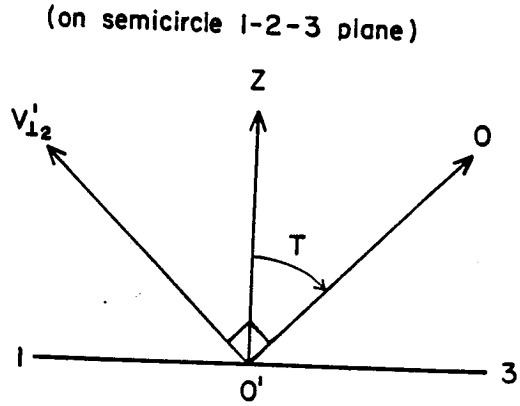

Fig. A-4-b

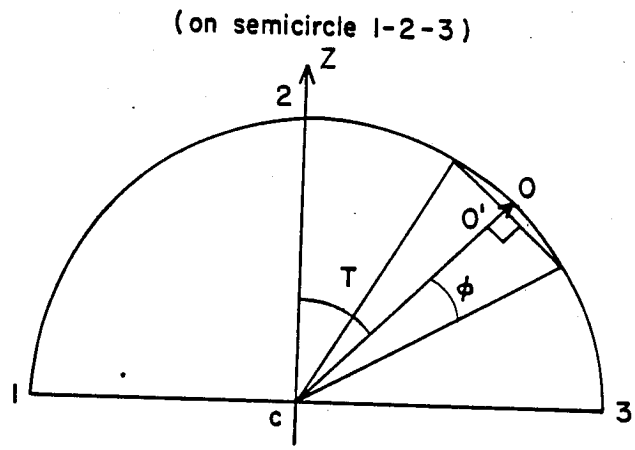

Fig. A-4-c

Fig. A-4

Thus, the total contribution in the x-direction is

$$[v']_x = v[\cos\phi \sin T \cos P + \sin\phi \sin\psi \sin P - \sin\phi \cos\psi \cos T \cos P]$$

and therefore

$$\Delta v_x = v'_x - v_x = v[-\sin\phi \cos\psi \cos T \cos P + \sin\phi \sin\psi \sin P - 2\sin^2(\phi/2) \sin T \cos P] \ .$$

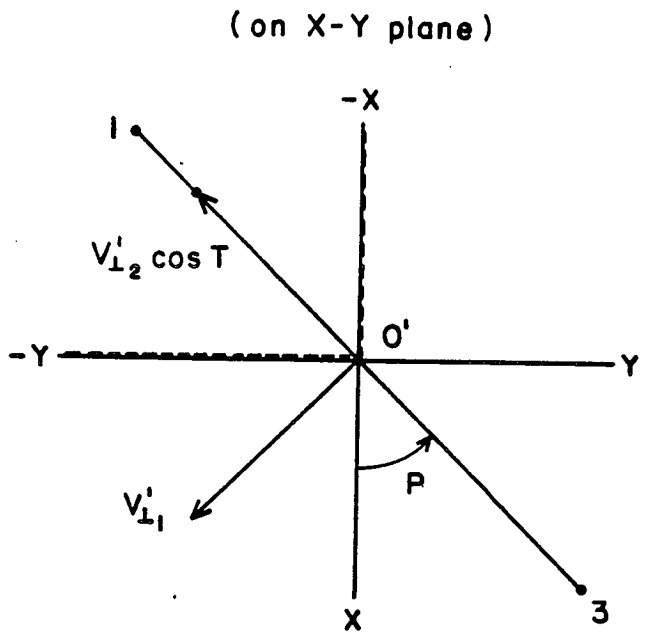

Fig. A-5

By a similar projection procedure for v'_y and v'_z we obtain

$$[\mathrm{v}']_\mathrm{y} = [\mathrm{v}'_{||}]_\mathrm{y} + [\mathrm{v}'_{\perp 1}]_\mathrm{y} + [\mathrm{v}'_{\perp 2}]_\mathrm{y} = v[\cos\phi \sin T \sin P + \sin\phi \sin\psi \cos P - \sin\phi \cos\psi \cos T \sin P]$$

and

$$\Delta v_y = v[-\sin\phi \cos\psi \cos T \sin P - \sin\phi \sin\psi \cos P - 2\sin^2(\phi/2) \sin T \sin P]$$

$$[\mathrm{v}']_\mathrm{z} = [\mathrm{v}'_{||}]_\mathrm{z} + [\mathrm{v}'_{\perp 2}]_\mathrm{z} = v[\cos\phi \cos T + \sin\phi \cos\psi \sin T]$$

$$\Delta v_z = v[\sin\phi \cos\psi \sin T - 2\sin^2(\phi/2) \cos T] \ .$$

By defining $\psi = -(\pi/2 + \psi_s)$ we arrive at the formulas used for the calculation of $\Delta\mathbf{v}$ in the particle code,

$$\Delta v_x = v[\sin\phi \sin\psi_s \cos T \cos P - \sin\phi \cos\psi_s \sin P - 2\sin^2(\phi/2) \sin T \cos P]$$

$$\Delta v_y = v[\sin\phi \sin\psi_s \cos T \sin P + \sin\phi \cos\psi_s \cos P - 2\sin^2(\phi/2) \sin T \sin P]$$

$$\Delta v_z = v[-\sin\phi \sin\psi_s \sin T - 2\sin^2(\phi/2) \cos T] \ .$$

References

1. C.Z. Cheng and H. Okuda, J. Comp. Phys. **25**, 133 (1977).

2. W.W. Lee and H. Okuda, J. Comp. Phys. **26**, 139 (1978).

3. R. Shanny, J.M. Dawson, and J.M. Greene, Phys. Fluids **10**, 1281 (1967).

4. J.F. Federici, W.W. Lee, and W.M. Tang, Phys. Fluids **30**, 425 (1987).

5. R.D. Sydora *et al.*, Phys. Fluids **28**, 255 (1985).

6. G. Rewoldt, W.M. Tang, and R.J. Hastie, Phys. Fluids **29**, 2893 (1986).

7. R.D. Sydora Ph.D. Thesis, Department of Physics, The University of Texas at Austin (1985); also Institute for Fusion Studies Report No. 178, The University of Texas at Austin (1985).

8. H. Naitou, S. Tokuda, and T. Kamimura, J. Comp. Phys. **38**, 265 (1980).

Figure Captions

1. Parallel velocity distribution of guiding-center electrons in case of ill-performed Lorentz collision operator. Ion velocity distributions remain essentially unchanged ($\nu_{ei} = 218\omega_e^*$ and taken at $t = 80\omega_{ci}^{-1}$).

2. Parallel electron and ion velocity distributions with implemented collisional procedure (same parameters as those of Fig. 1).

3. Linear growth rate and real frequency of electrostatic resistive interchange mode for each m mode versus collision frequency. Note growth rate and collision frequency are normalized to the diamagnetic drift frequency ω_e^* for mode $m = 1$.

4. Comparison of the measured simulation growth rate for the resistive interchange mode with the linear theory result $\gamma \sim \nu_{ei}^{1/3}$.

5. Bounded $2-\frac{1}{2}$ D sheared slab model for simulation. Density gradient is in the negative x-direction and centrifugal force mg is in the positive x-direction in sheared slab. The mode rational surface is located in the middle of the system at $x_0 = L_x/2$.

6. Electron and ion density profiles in the saturated state for the cases with $\nu_{ei} = 0, 80$ and $160\omega_e^*$.

7. Global electrostatic energy, $|E_L|^2 = \sum_k k^2|\Phi_k|^2$ normalized by electron kinetic energy $4\pi n_0 T_e$ versus time for the same cases as in Fig. 6.

8. Comparison of linear growth rate between simulation and theory for the $m = 3$ mode, which is the most dominant mode in simulation. Higher wave numbers above $m = 3$ are affected by finite size particle effects and are less dominant.

9. Mode structure comparison between simulation and theory. Both simulation and theory grids extend up to $16\,\rho_i$ from the mode rational surface.

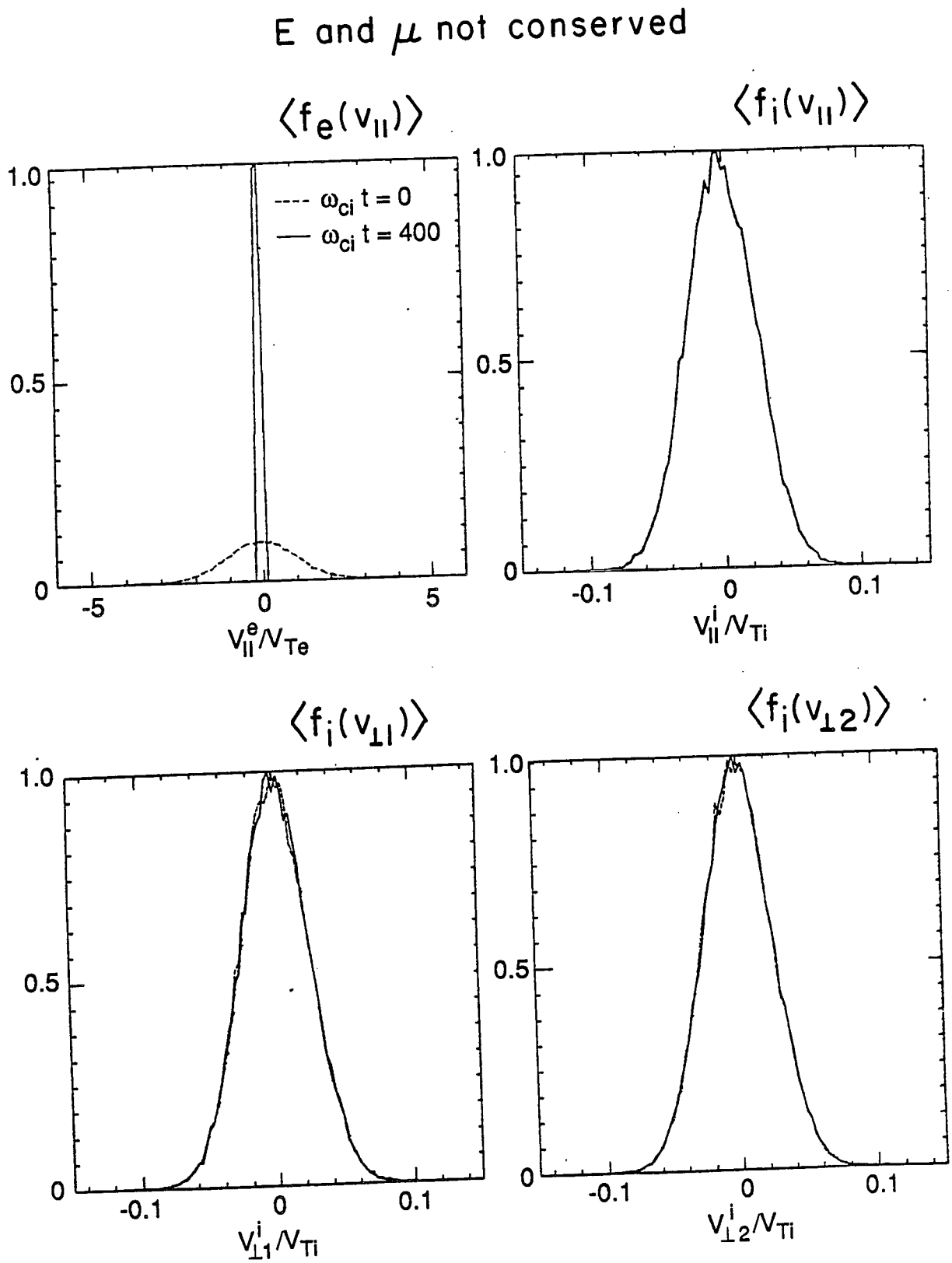
E and μ not conserved
⟨f_e(v_∥)⟩
---- ω_ci t = 0
— ω_ci t = 400
1.0
0.5
0
-5
0
5
V_∥^e/V_Te
⟨f_i(v_∥)⟩
1.0
0.5
0
-0.1
0
0.1
V_∥^i/V_Ti
⟨f_i(v_⊥1)⟩
1.0
0.5
0
-0.1
0
0.1
V_⊥1^i/V_Ti
⟨f_i(v_⊥2)⟩
1.0
0.5
0
-0.1
0
0.1
V_⊥2^i/V_Ti

Fig. 1

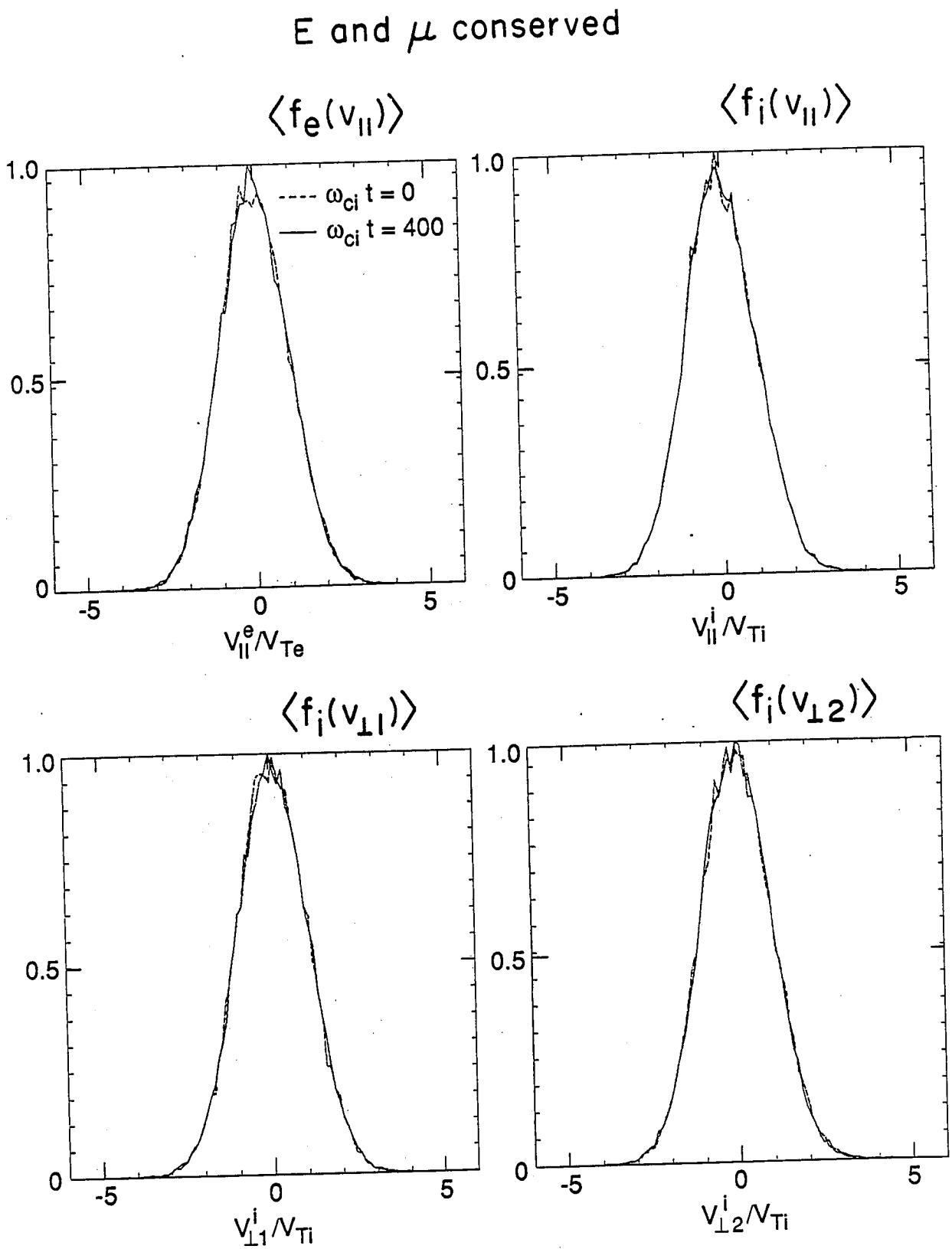
E and μ conserved
⟨f_e(v_∥)⟩
⟨f_i(v_∥)⟩
⟨f_i(v_⊥1)⟩
⟨f_i(v_⊥2)⟩
---- ω_ci t = 0
—— ω_ci t = 400
1.0
0.5
0
-5
0
5
V_∥^e/V_Te
V_∥^i/V_Ti
V_⊥1^i/V_Ti
V_⊥2^i/V_Ti

Fig. 2

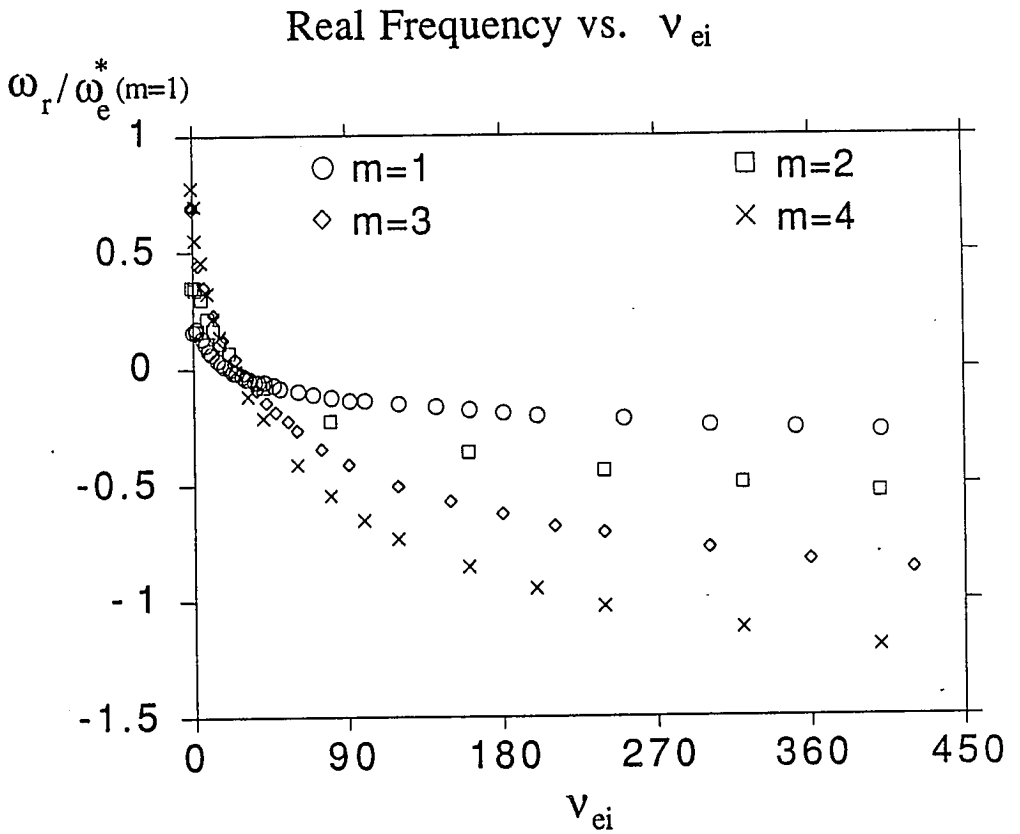
Real Frequency vs. ν_{ei}
$\omega_r / \omega_e^*(m=1)$
1
0.5
0
-0.5
-1
-1.5
0
90
180
270
360
450
ν_{ei}
m=1
m=2
m=3
m=4

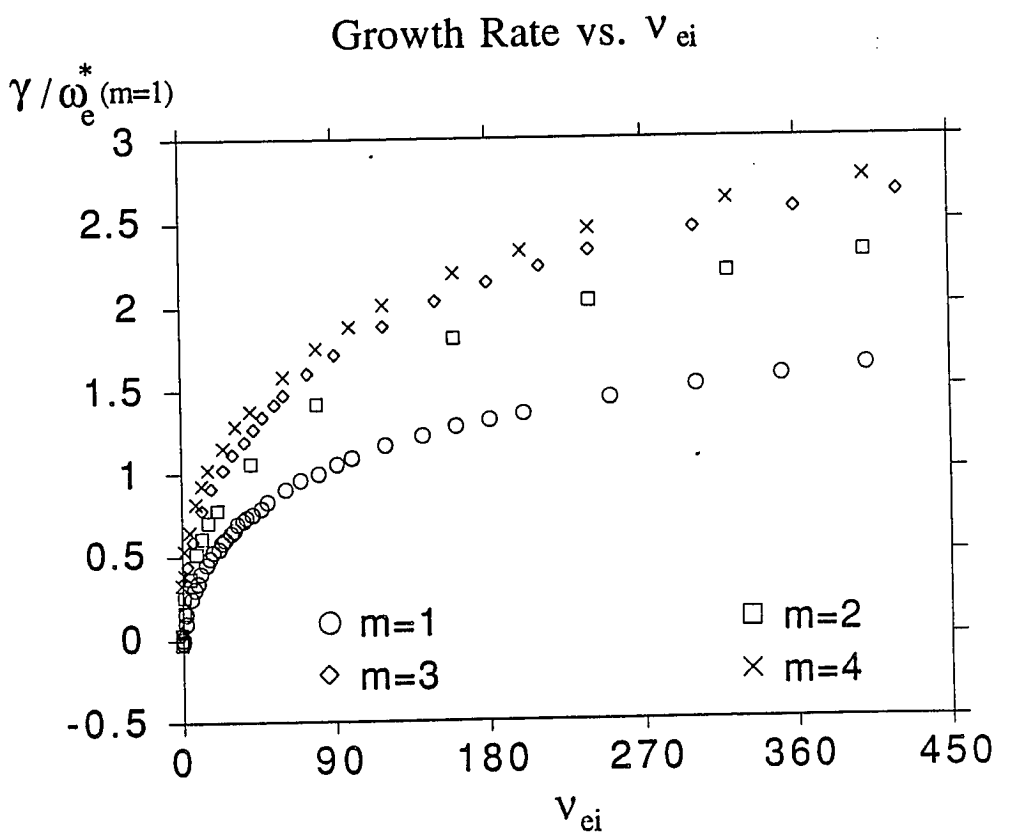
Growth Rate vs. ν_{ei}
$\gamma / \omega_e^*(m=1)$
3
2.5
2
1.5
1
0.5
0
-0.5
0
90
180
270
360
450
ν_{ei}
m=1
m=2
m=3
m=4

Fig. 3

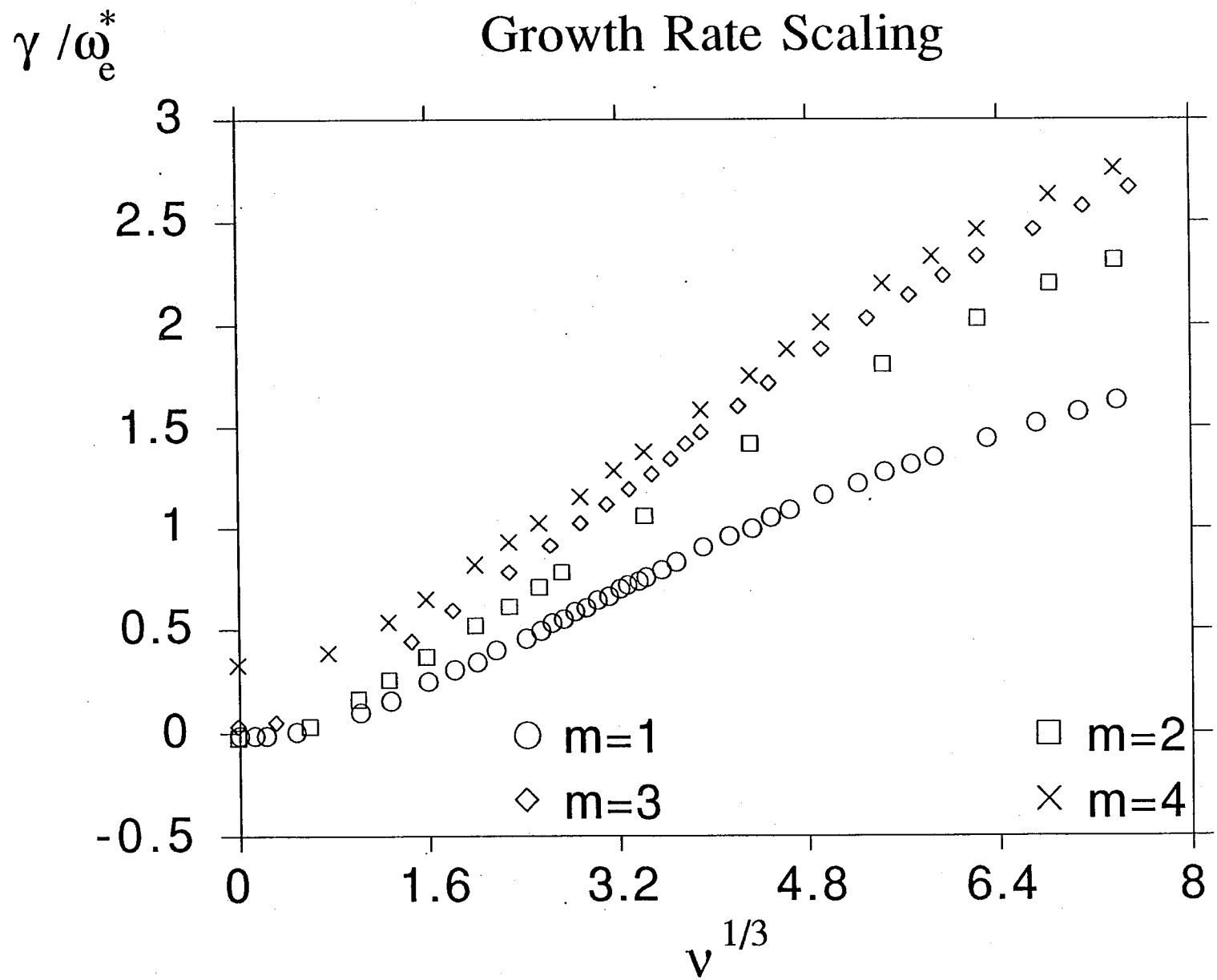
Growth Rate Scaling
γ / ω_e^*
3
2.5
2
1.5
1
0.5
0
-0.5
0
1.6
3.2
4.8
6.4
8
$\nu^{1/3}$
m=1
m=2
m=3
m=4

Fig. 4

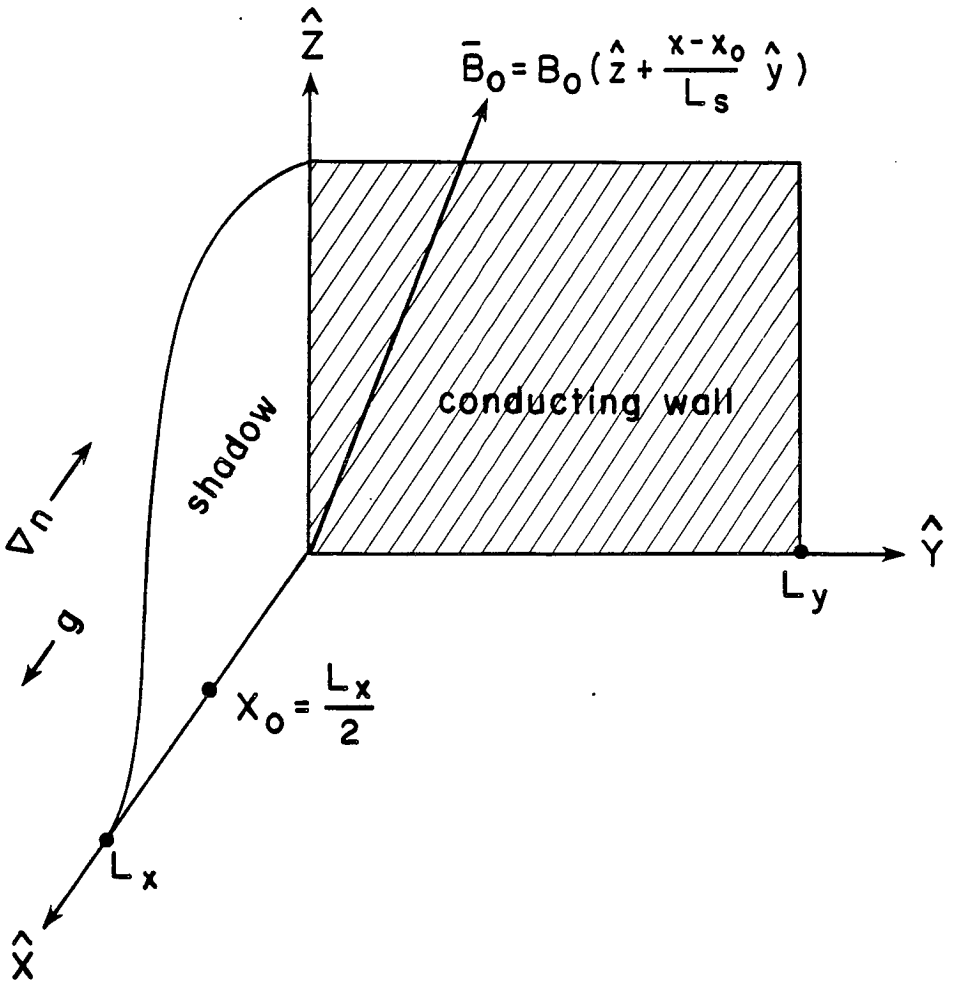
$\hat{Z}$
$\bar{B}_0 = B_0 (\hat{z} + \frac{x - x_0}{L_s} \hat{y})$
conducting wall
shadow
∇n
g
$\hat{Y}$
L_y
$X_0 = \frac{L_x}{2}$
L_x
$\hat{X}$

Fig. 5

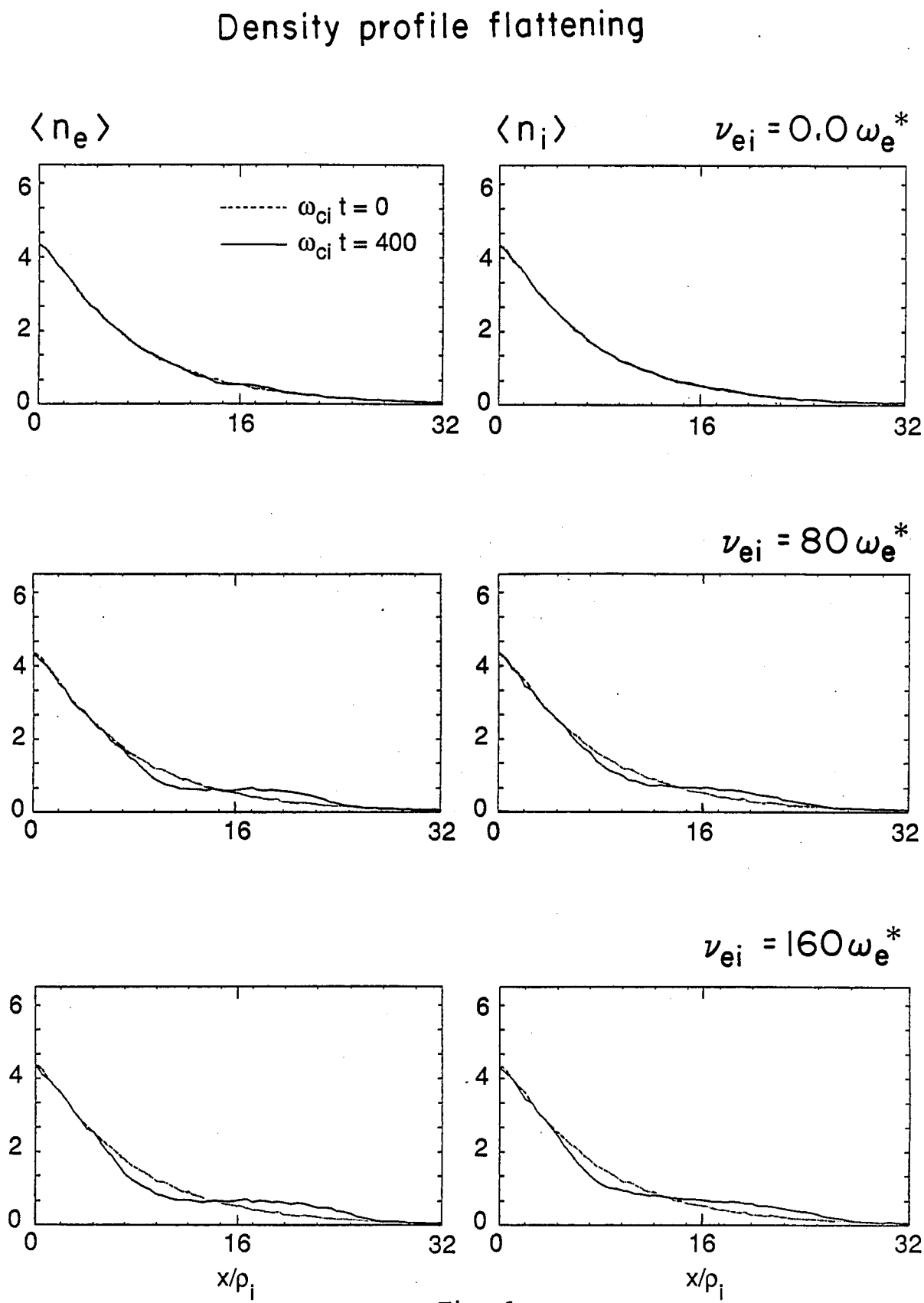
Density profile flattening
⟨n_e⟩
⟨n_i⟩
ν_ei = 0.0 ω_e*
ω_ci t = 0
ω_ci t = 400
ν_ei = 80 ω_e*
ν_ei = 160 ω_e*
0
2
4
6
0
16
32
x/ρ_i

Fig. 6

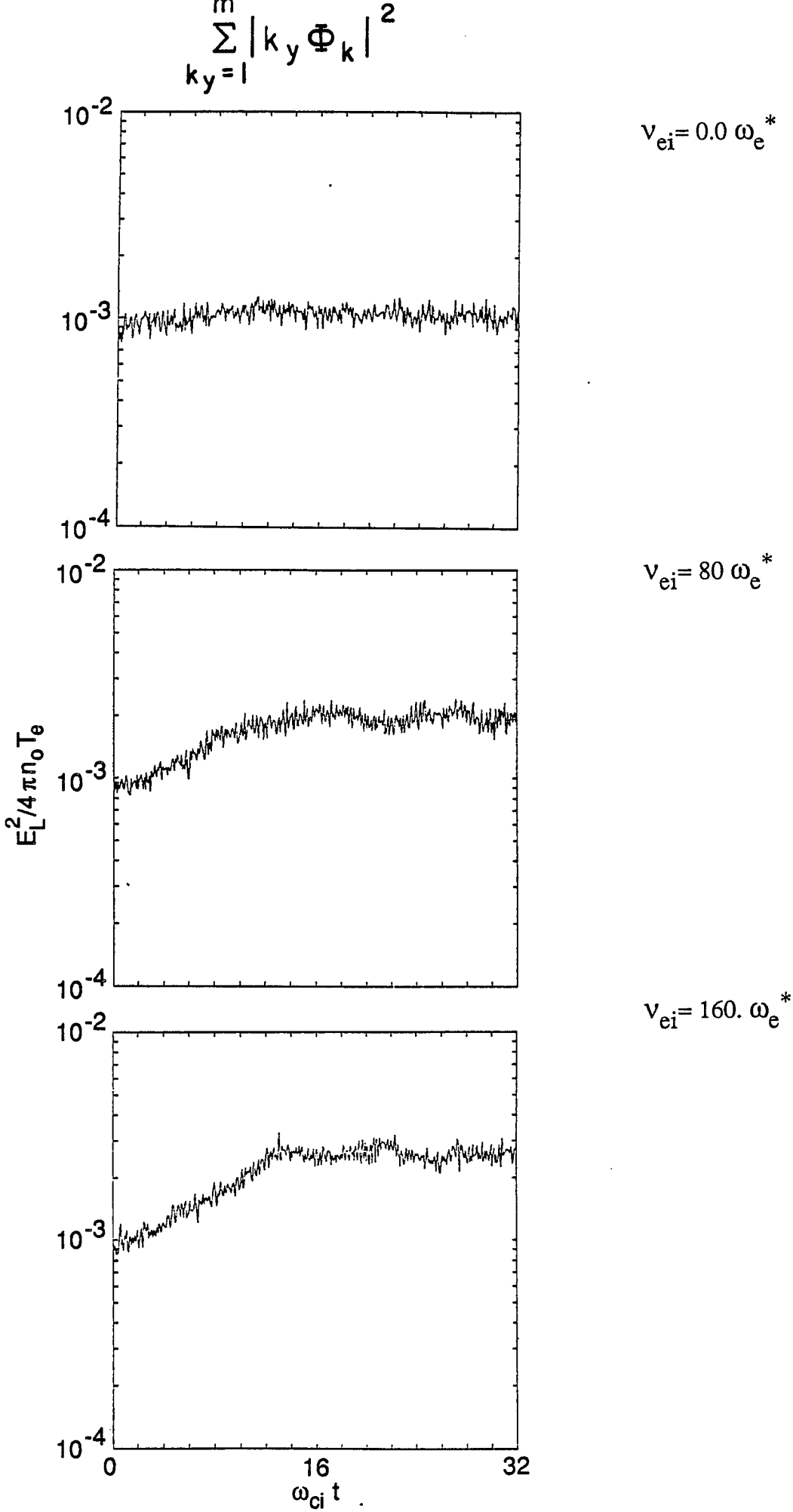
$\sum_{k_y=1}^{m} |k_y \Phi_k|^2$
10^{-2}
10^{-3}
10^{-4}
$\nu_{ei} = 0.0\ \omega_e^*$
$\nu_{ei} = 80\ \omega_e^*$
$\nu_{ei} = 160.\ \omega_e^*$
$E_L^2/4\pi n_o T_e$
0
16
32
$\omega_{ci}\ t$

Fig. 7

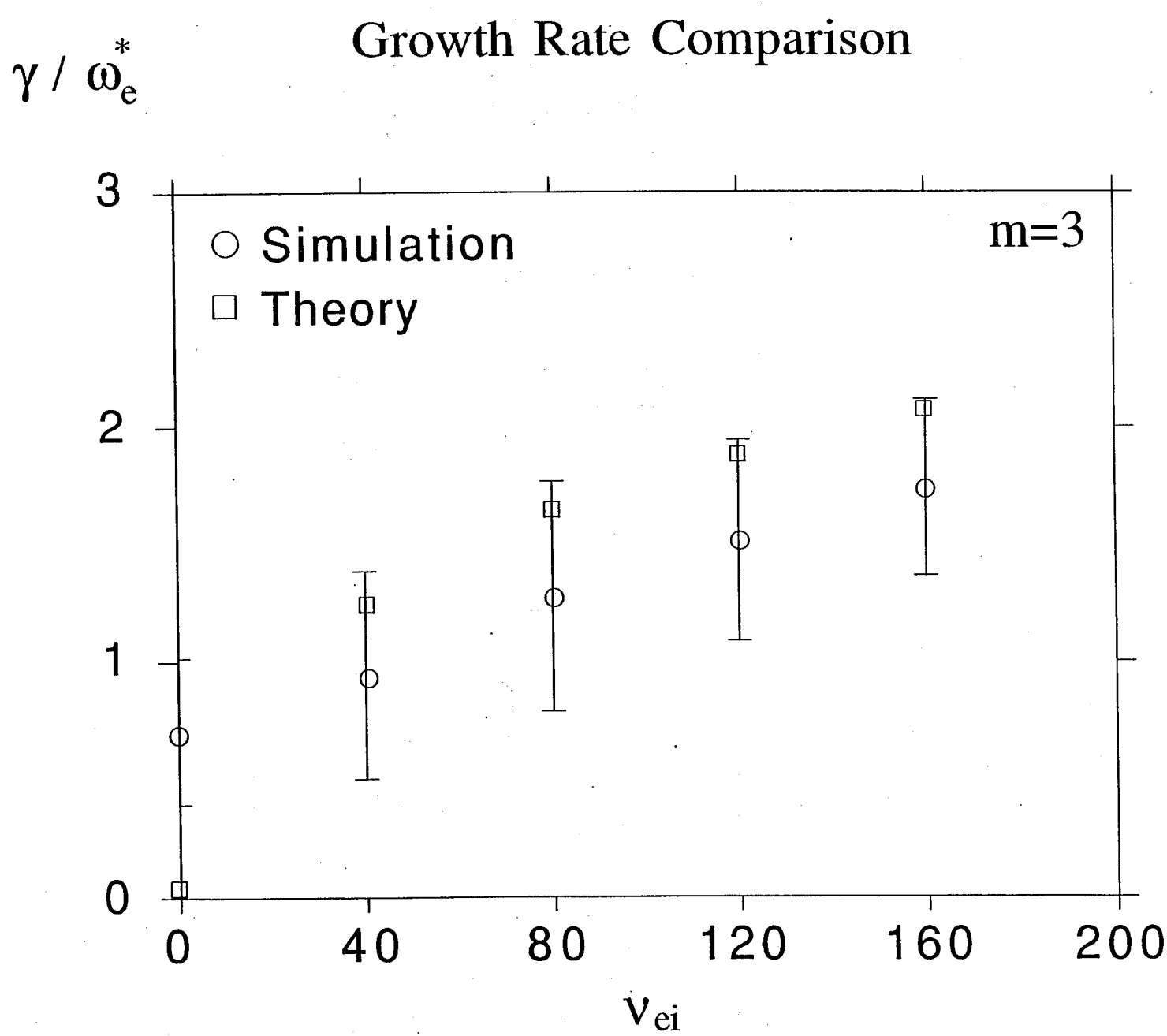
Growth Rate Comparison
γ / ω_e^*
Simulation
Theory
m=3
3
2
1
0
0
40
80
120
160
200
ν_{ei}

Fig. 8

Mode Structure Comparision

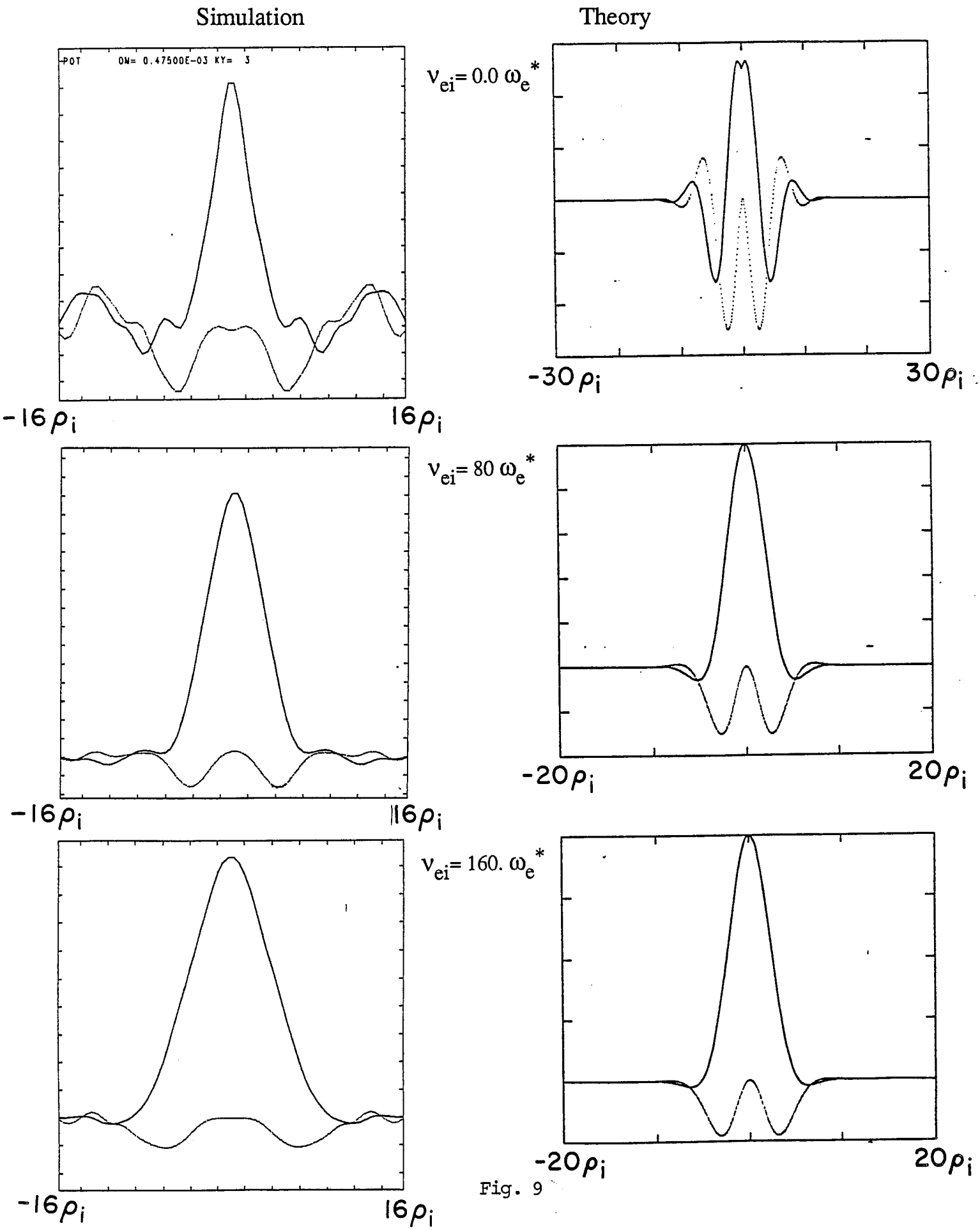

Fig. 9